

Incorporation of Endosomolytic Peptides with Varying Disruption Mechanisms into EGFR-Targeted Protein Conjugates: The Effect on Intracellular Protein Delivery and EGFR Specificity in Breast Cancer Cells

Rachel M. Lieser, Qirun Li, Wilfred Chen,* and Millicent O. Sullivan*



Cite This: *Mol. Pharmaceutics* 2022, 19, 661–673



Read Online

ACCESS |



Metrics & More



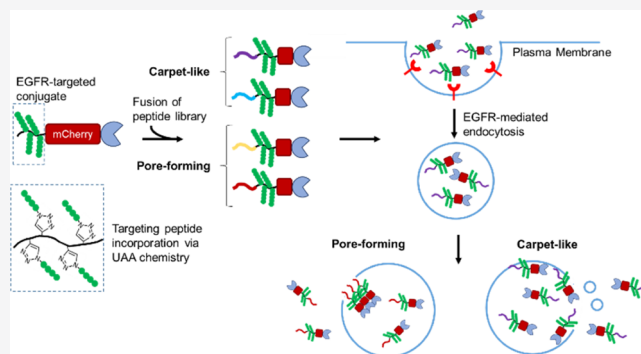
Article Recommendations



Supporting Information

ABSTRACT: Intracellular delivery of protein therapeutics remains a significant challenge limiting the majority of clinically available protein drugs to extracellular targets. Strategies to deliver proteins to subcellular compartments have traditionally relied on cell-penetrating peptides, which can drive enhanced internalization but exhibit unreliable activity and are rarely able to target specific cells, leading to off-target effects. Moreover, few design rules exist regarding the relative efficacy of various endosomal escape strategies in proteins. Accordingly, we developed a simple fusion modification approach to incorporate endosomolytic peptides onto epidermal growth factor receptor (EGFR)-targeted protein conjugates and performed a systematic comparison of the endosomal escape efficacy, mechanism of action, and capacity to maintain EGFR-targeting specificity of conjugates modified with four different endosomolytic sequences of varying modes of action (Aurein 1.2, GALA, HA2, and L17E). Use of the recently developed Gal8-YFP assay indicated that the fusion of each endosomolytic peptide led to enhanced endosomal disruption. Additionally, the incorporation of each endosomolytic peptide increased the half-life of the internalized protein and lowered lysosomal colocalization, further supporting the membrane-disruptive capacity. Despite this, only EGFR-targeted conjugates modified with Aurein 1.2 or GALA maintained EGFR specificity. These results thus demonstrated that the choice of endosomal escape moiety can substantially affect targeting capability, cytotoxicity, and bioactivity and provided important new insights into endosomolytic peptide selection for the design of targeted protein delivery systems.

KEYWORDS: EGFR, targeted delivery, intracellular protein delivery, endosomolytic peptides



1. INTRODUCTION

Delivering protein therapeutics into cells remains a major obstacle. Proteins require active strategies to cross the cell membrane for internalization. Additionally, proteins are often uptaken through endocytosis, and so accessing the cytosol or other subcellular compartments requires internalized proteins to escape the endosome to evade lysosomal degradation or exocytosis.¹ Because of these challenges, intracellular proteins make up less than 5% of protein therapeutics entering clinical development,² yet they remain of immense interest due to their therapeutic potential and capacity to treat “undruggable” targets for a multitude of diseases.^{3,4} Proteins also have shown promise as carriers for other cargoes, including small-molecule drugs^{5,6} and nucleic acids (e.g., RNA^{7,8} and DNA^{9,10}), which often require cytosolic or nuclear targeting.

Past efforts to deliver proteins to intracellular targets have commonly relied on cationic cell-penetrating peptides (CPPs), which can enhance cellular uptake as compared with unmodified proteins, but often exhibit inadequate cell

specificity, cytotoxicity, and poor *in vivo* activity.¹ For example, Tat,¹¹ a cationic peptide derived from HIV-1, has been tested in various preclinical analyses as a means to improve the intracellular delivery of various biologics.^{12,13} However, the mechanism of Tat internalization and its effectiveness at transporting cargo to the cytosol remains highly disputed in the literature, with results varying greatly between cell types and cargoes.^{1,14–19} *In vivo* delivery poses additional challenges regarding stability, biodistribution, and immunogenicity. Tat fused to an antiapoptotic regulator, c-FLIP, successfully inhibited tumor growth *in vivo*;²⁰ however, a recent clinical trial for an α -PKC inhibitor fused to Tat, known as delcasertib,

Received: October 15, 2021

Revised: January 5, 2022

Accepted: January 6, 2022

Published: January 18, 2022



failed to show a significant improvement in myocardial injury.²¹ Together, these examples demonstrate that while Tat works for some applications, its behavior is context-dependent and cannot be generalized.

To combat the cytotoxicity and cell specificity issues surrounding cationic CPPs, pH-responsive endosomolytic peptides have been engineered to disrupt the endosome by fusing with the membrane following a pH-triggered conformational change.²² These peptides exhibit lytic properties in the acidic environment of the endosome but not in the pH-neutral extracellular environment. A majority of these pH-responsive endosomolytic peptides disrupt the endosomal membrane through one of two mechanisms: the pore-forming mechanism, also known as the barrel-stave mechanism, and the carpet-like mechanism.²³ It has been hypothesized that peptides that utilize the carpet-like mechanism have greater endosomolytic activity than pore-forming peptides, but a direct comparison of these peptides within the same delivery system has not been performed.²⁴

In the pore-forming mechanism, neutral or negatively charged amphiphilic peptides form an α -helix at low pH that allows the monomers to bind to the membrane and insert into the bilayer so that the hydrophobic residues align with the core of the membrane.²⁵ The pore size increases as more peptide monomers are recruited, forming pores that are typically no larger than 10 nm in diameter.^{26–28} One of the most commonly used synthetic endosomolytic peptides, GALA, uses the pore-forming mechanism.²⁹ GALA, a 30-amino acid synthetic peptide made up of glutamic acid-alanine-leucine-alanine (EALA) repeats, carries a high negative charge at neutral pH due to the carboxylic acid moieties of the Glu residues, which destabilize its secondary structure through electrostatic repulsion. At acidic pH, the Glu side chains protonate, increasing their hydrophobicity, and GALA forms an amphiphilic α -helical structure capable of interacting with and disrupting lipid bilayers. Virus-derived peptides also commonly utilize this mechanism, including hemagglutinin-2 (HA2) derived from the influenza virus,³⁰ and HGP derived from the endodomain of HIV gp41.^{31,32}

In the carpet-like mechanism, cationic amphiphilic peptides electrostatically bind and cover the lipid membrane, with the hydrophobic residues facing the membrane surface.³³ Above a critical concentration, the peptides are thought to collapse the lipid membrane, leading to micellization. Pores formed by peptides employing the carpet-like pore-forming mechanism are typically significantly larger than those formed by peptides utilizing the pore-forming mechanism. For example, in the case of the lytic peptide from the flock house virus, holes of 50–500 nm are formed in the endosomal membrane.³⁴ Antimicrobial peptides also frequently use the carpet-like mechanism to access the cytosol.³⁵ One such antimicrobial peptide, Aurein 1.2, has demonstrated pH-sensitive endosomolytic activity in mammalian cells.^{36,37} The engineered antimicrobial peptide, L17E, also utilizes the carpet-like mechanism. L17E was engineered from M-lycotoxin by substituting a leucine with glutamic acid to attenuate its lytic activity at neutral pH.³⁸

Endosomolytic peptides have shown significant promise in nanoparticle systems, enabling a variety of cargoes to be successfully delivered to the cytosol.^{39–42} Recently, GALA-functionalized mRNA polyplexes encoding for OVA enhanced T-cell responses and stimulated dendritic cell maturation, demonstrating potential as an mRNA-based vaccine platform.⁴³ In another example, L17E was able to facilitate the

knockdown of mRNA levels by ~50% when conjugated to the surface of cowpea chlorotic mottle virus nanoparticles loaded with siRNA.⁴⁴ While these endosomolytic peptides have shown promise in nanoparticle systems, only a handful of them have been fused to therapeutic proteins and tested for intracellular protein delivery.^{36,38,45} To understand the full potential of endosomolytic peptides for protein delivery, further studies are necessary to generalize their use for delivering proteins that vary in size and composition.

We previously developed an epidermal growth factor receptor (EGFR)-targeted protein conjugate capable of delivering a prodrug-converting enzyme for robust, cell-specific breast cancer treatment.⁴⁶ Clustering four EGFR ligands onto the target protein through unnatural amino acid (UAA) incorporation resulted in significantly higher cellular internalization than a Tat fusion protein, and this ligand modification approach also elevated prodrug conversion activity. However, the intracellular half-life of the internalized protein was limited by entrapment in the endosome, leading to protein degradation within 16 h. While this was not detrimental for the delivery of a prodrug-converting enzyme due to the membrane permeability of both the substrate and product, cargoes that function in the cytosol or other subcellular compartments require endosomal escape.

To make our EGFR-targeted protein conjugate amenable to a variety of intracellularly active cargoes, four endosomolytic peptides with differing mechanisms of endosomal disruption (e.g., peptides utilizing both the pore-forming and the carpet-like mechanisms) were incorporated into the conjugate to promote endosomal escape. Two peptides that disrupt the endosome through the pore-forming mechanism, GALA²⁵ and HA2,³² and two peptides that use the carpet-like mechanism, Aurein 1.2³⁶ and L17E,³⁸ were tested for their ability to disrupt the endosome when fused to the N-terminus of the conjugate. Our results demonstrated that L17E was not sufficiently amenable to genetic fusion, resulting in poor expression yields and high cytotoxicity. Additionally, while HA2 was highly efficient at disrupting the endosomal compartment, it acted as a non-cell-specific CPP. Only the Aurein 1.2 and GALA peptides were able to improve the endosomal escape of the EGFR-targeted conjugate while also maintaining specificity toward EGFR-overexpressing cells. Together, these results highlight both the importance of endosomolytic peptide selection when designing targeted protein delivery systems and the versatility of our EGFR-targeted conjugate for intracellular delivery.

2. MATERIALS AND METHODS

2.1. Reagents and Materials. DNA oligos were all purchased from IDT (Coralville, IA). Restriction enzymes, T4 polynucleotide kinase (PNK), and T4 DNA ligase for DNA cloning were purchased from NEB (Ipswich, MA). Ingredients for bacterial culture medium were purchased from Fisher Scientific (Pittsburgh, PA). Plasmid and gel extraction kits were purchased from Zymo Research (Irvine, CA) for DNA purification following digestion or gel electrophoresis. Isopropyl- β -D-1-thiogalactopyranoside (IPTG) and antibiotics were purchased from Sigma-Aldrich (St. Louis, MO). The UAA, *p*-azido-L-phenylalanine (4-azido-L-phenylalanine, >98% (HPLC)), was purchased from Chem-Impex International Inc. (Wood Dale, IL). Sodium dodecyl sulfate-polyacrylamide gel electrophoresis (SDS-PAGE) reagents were purchased from BIO-RAD (Hercules, CA). Amino acids and resin used for

synthesizing GE11 were purchased from MilliporeSigma (Burlington, MA) and CEM Corporation (Matthews, NC), respectively. Solvents used for peptide synthesis were purchased from Fisher Chemical (Fair Lawn, NJ). Dulbecco's phosphate-buffered saline (DPBS, 1×), Ham's F-12, and Dulbecco's modification of Eagle's medium/Ham's F-12 50/50 Mix and Dulbecco's modification of Eagle's medium (DMEM) were purchased from Thermo Fisher Scientific (Grand Island, NY).

2.2. Construction of Expression Plasmids. Constructs were prepared using standard molecular cloning techniques. Gene fragments encoding Aurein 1.2, GALA, HA2, and L17E were annealed using their corresponding forward and reverse primers (Section 2.1 in the Supporting Information) followed by T4 polynucleotide kinase treatment. The DNA fragments were inserted into pET22b-4amber-mCherry-SpyCatcher-his6⁴⁶ using *NdeI* and *NotI* sites to yield the endosomal lytic peptide fusion proteins. Additionally, a *KpnI* cut site was incorporated into all of the constructs for colony screening. All plasmids were transformed into *Escherichia coli* NEB5 α (NEB, Ipswich, MA) [*fhuA2* Δ (*argF-lacZ*)U169 *phoA* 23 *glnV44* Φ 80 Δ (*lacZ*)M15 *gyrA96* *recA1* *relA1* *endA1* *thi-1* *hsdR17*]. Bacteria were grown on 15 g/L agar and 25 g/L Luria-Bertani broth (LB, 10 g/L tryptone, 5 g/L yeast extract, 5 g/L sodium chloride) plates supplemented with 100 μ g/mL ampicillin. Positive clones were confirmed by DNA sequencing, and the positive clones were cotransformed with pULTRA-CNF (a gift from Prof. Peter G. Schultz⁴⁷) into *E. coli* strain BL21(DE3) (EMD Millipore, Madison, WI) [*F-ompT* *hsdSB*(*rB*-*mB*-) *gal dcm* (DE3) Δ (*srhA*)306::Tn10 (*TetR*)] on plates supplemented with 100 μ g/mL ampicillin and 100 μ g/mL spectinomycin. Primers and plasmid sequences are available in the Supporting Information (Sections 2.1 and 2.3).

2.3. Expression and Purification of Proteins. Proteins were expressed in terrific broth (TB) media (12 g/L tryptone, 24 g/L yeast extract, 0.4% (v/v) glycerol, 9.4 g/L monopotassium phosphate, 2.2 g/L dipotassium phosphate) supplemented with 100 μ g/mL ampicillin and 100 μ g/mL spectinomycin. Cultures were inoculated with a 3.5 mL culture started from a single colony to an OD₆₀₀ of 0.05 and allowed to grow at 37 °C in a shake flask to an OD₆₀₀ of 0.6–0.8. The 4pAzF-mCherry-SpyCatcher fusion constructs were induced with 1 mM IPTG and supplemented with 4 mM pAzF then grown at 37 °C for 15–18 h. 0pAzF-mCherry-SpyCatcher fusions, without pAzF, were induced with 100 μ M IPTG and grown overnight at 25 °C for 15–18 h.

Cells were pelleted with centrifugation at 4000g for 10 min at 4 °C. Spent media was removed, and cells were resuspended in 1× phosphate-buffered saline (PBS, pH 7.4) with 10 mM imidazole to an OD₆₀₀ of 25. Cells were lysed via sonication and centrifuged at 10 000g for 15 min at 4 °C to collect soluble protein. The insoluble protein pellet was saved and run on an SDS-PAGE gel. Proteins were purified using His-Bind Ni-NTA resin gravity column from Thermo Fisher (Pittsburgh, PA) according to the manufacturer's protocol. After purification, proteins were dialyzed overnight in 1× PBS. Each protein, with and without 4pAzF, contains a C-terminal truncation (~28 kDa) within the mCherry sequence that could not be removed with His-tag purification, making up approximately 20% of the final product. The truncation does not contain the active peptides and so should not impact the results of this study as 0GE11-mCherry-SC shows no activity in any of the studies. Densitometry was used to determine the percent of truncation

in the sample to determine the concentration of active full-length proteins more accurately.

2.4. Synthesis of GE11 Peptide. The protocol for synthesizing GE11 and performing the corresponding MALDI-TOF mass spectrometry is detailed in our previous work.⁴⁶ Briefly, GE11 with an N-terminal linker (HAIYPR-HYHWYGYTPQNVI) was synthesized via solid-phase peptide synthesis. Fmoc-L-propargylglycine was added to the N-terminus to incorporate an alkyne group into the peptide for reaction with the pAzF-incorporated protein. The peptide was purified via reverse-phase high-performance liquid chromatography, and the final product was confirmed by MALDI-TOF mass spectrometry.

2.5. Site-Specific Conjugation of GE11 Peptide to Proteins. Copper-catalyzed alkyne–azide cycloaddition (CuAAC) was used to conjugate GE11 to mCherry constructs. Briefly, 60 μ M alkyne-GE11 was reacted to 15 μ M X-4AzmCherry-SC in 1× PBS (pH 7.4) with 250 μ M CuSO₄, 1.25 mM THPTA ligand, and 5 mM sodium ascorbate for 1 h at room temperature. The protein-peptide conjugates were then purified with His-Bind Ni-NTA resin to remove unreacted GE11 and copper ions, and the proteins were dialyzed overnight in 1× PBS. The products were analyzed with SDS-PAGE. Samples were filtered with a 0.22 μ M syringe filter prior to use in cellular analyses.

2.6. Cell Culture. IBC SUM149 cells (a gift from Prof. Kenneth van Golen⁴⁸) were grown in Ham's F-12 medium supplemented with 5% FBS, 1% (v/v) mycoplasma antibiotic supplement, 1% (v/v) penicillin/streptomycin, 1% (v/v) glutamine, 5 μ g/mL insulin, 2.5 μ g/mL transferrin, 200 ng/mL selenium, and 1 μ g/mL hydrocortisone according to previously established methods. MCF10A cells were grown in 50/50 DMEM/Ham's F-12 medium supplemented with 5% FBS, 1% (v/v) penicillin/streptomycin, 50 μ g/mL bovine pituitary extract, 10 μ g/mL insulin, 0.5 μ g/mL hydrocortisone, 100 ng/mL cholera toxin, and 20 ng/mL epidermal growth factor. MDA-MB-231 cells stably expressing Galectin8-YFP (a gift from Prof. Craig L. Duvall⁴⁹) were grown in DMEM medium supplemented with 10% FBS and 0.1% (v/v) gentamicin.

2.7. Cellular Internalization of Proteins. IBC SUM149 cells, MCF10A cells, or MDA-MB-231 cells were seeded (6 × 10⁴ cells/well) in 8-well Lab-Tek Chambered Cover Glass plates with a collagen film (1.5 mg/mL Collagen I Bovine Protein in 0.02 M acetic acid in deionized water) and incubated overnight at 37 °C. Cells were then incubated with 1 μ M of protein for 3 h. The media were removed, and cells were washed three times in 1× DPBS to remove the unbound protein. Cells were then fixed with 10% formalin for 15 min, treated with DAPI (300 nM) for 10 min, and rinsed twice with 1× DPBS. Internalization was observed on a Leica DM6000 fluorescence microscope (Wetzlar, Germany) with a 40× objective. Images were taken using 350/50 nm excitation and 460/50 nm emission for DAPI and 545/25 nm excitation and 605/70 nm emission for mCherry.

Flow cytometry was used as a quantitative analysis of mCherry association in IBC SUM149 and MCF10A cells. Cells were seeded in 12-well cell culture-treated plates at a density of 1.5 × 10⁵ cells/well and incubated overnight at 37 °C. The medium was replaced, and cells were incubated with 1 μ M of protein for 3 h. Cells were washed three times in 1× DPBS before being treated with trypsin. Cells were subsequently neutralized with the appropriate cell media and centrifuged at

Table 1. List of the Endosomolytic Peptides Used in This Study with Their Amino Acid Sequence, Net Charge at pH 7, and Mechanism of Action

peptide	sequence	net charge (pH 7)	mode of action
Aurein 1.2	GLFDIHKIAESF	0	carpet-like
GALA	WEAALAEALAEALAEHLAEALAEALAA	−6.9	pore-forming
HA2	GDIMGEWGNEIFGAAGFLGC	−3.1	pore-forming
L17E	IWLTKLFLGKHAAKHEAKQQLSKL	4.2	carpet-like

123g for 4 min. Cells were resuspended in cold 1× DPBS, put through a cell strainer, and analyzed with flow cytometry (NovoCyte, ACEA Biosciences, Inc., San Diego, CA). The mCherry fluorescence intensity of 1.5×10^4 cells was measured with a 488 nm excitation laser at an emission wavelength of 660 nm.

2.8. Lysosomal Degradation. The 0 h samples were prepared as described in Section 2.7. For the 16 h samples, 6×10^4 IBC SUM149 cells were seeded in 8-well plates coated with a collagen film and incubated overnight at 37 °C. Cells were then incubated with 1 μ M of protein for 3 h, washed 3× with DPBS to remove extracellular protein, and incubated at 37 °C for an additional 16 h. After 16 h, cells were fixed, stained with DAPI, and imaged as described.

For flow cytometry experiments, cells were seeded in 12-well cell-treated plates at a density of 1.5×10^5 cells/well and incubated overnight at 37 °C. The next day, cells were incubated with protein for 3 h, washed 3× with DPBS, and incubated at 37 °C for 16 h. After 16 h, the cells were prepped for flow cytometry as described above and the mCherry fluorescence intensity of 1.5×10^4 cells was measured with the NovoCyte flow cytometer. For chloroquine (CQ)-containing samples, cells were treated with 100 μ M of chloroquine for 4 h before being treated with 1 μ M of 4GE11-mCherry-SC and processed for analysis, as described.

2.9. Lysosomal Colocalization. IBC SUM149 cells were seeded on a collagen-coated 8-well glass plate as described above before being incubated at 37 °C overnight. Cells were subsequently incubated with 1 μ M of protein for 3 h, washed 3 times with 1× DPBS, and covered in media before being returned to the incubator for 10 h. Next, cells were stained with 150 nM LysoView (Biotium, Fremont, CA) in cell medium and NucBlue LiveReadyProbes Reagent (Hoechst 33342) (Thermo Fisher Scientific, Grand Island, NY) for 30 min. The medium was removed, and cells were resuspended in Live Cell Imaging Solution before being imaged with a Zeiss LSM 880 confocal microscope (Thornwood, NY). Zeiss colocalization software was used to measure Mander's correlation coefficient (M_r).

2.10. Galectin8-YFP (Gal8-YFP) Endosomal Disruption Assay. MDA-MB-231 cells expressing Gal8-YFP were seeded in an 8-well Lab-Tek Chambered Cover Glass plate coated with a collagen film at a density of 5×10^4 cells/well and incubated overnight at 37 °C. Cells were incubated with 1 μ M of protein for 3 h. The medium was removed, and cells were washed three times in 1× DPBS. Next, fresh medium was added to the cells and the cells were incubated for 16 additional h. After incubating, the medium was removed, and cells were fixed as described above. The cells were visualized with a 40× objective on a Leica DM6000 fluorescence microscope (Wetzlar, Germany) with 350/50 nm excitation and 460/50 nm emission for DAPI and 488/40 nm excitation and 525/50 nm emission for YFP.

2.11. Gal8-YFP Quantification. To quantify the Gal8-positive puncta normalized to cell number, the MATLAB code generated by Kilchrist et al.⁵⁰ was adapted for images taken on a Leica microscope with a 40× objective. Briefly, thresholding was used to identify Gal8-positive puncta, and a visual check was outputted in which Gal8-positive puncta were identified with red circles. The program also counted the number of DAPI-stained nuclei in each image and outputted a visual check to ensure each nucleus in the image was counted. The program then calculated the sum of Gal8-positive puncta intensity normalized to the number of cells in each image. This calculation was done for at least 15 images from three independent experiments for each sample. An example of the Gal8-YFP quantification visualization checks is provided in the Supplemental Information (Figure S10). The derivative code used here is available on the Figshare platform at <https://doi.org/10.6084/m9.figshare.16803625.v1>.⁵¹

2.12. Cell Viability Analysis. IBC SUM149 cells were seeded in a tissue culture-treated 96-well plate (Corning Inc., Corning, NY) at a density of 2×10^4 cells/well and incubated overnight. Ham's F-12 media with 2 μ M of protein was added to the cells and incubated for 3 h. Following incubation, cells were washed 2× with DPBS to remove extracellular protein and resuspended in fresh media. After 72 h of incubation at 37 °C, cells were incubated with a second dose of 2 μ M of protein for 3 h and washed before replacing the media. Cells were then allowed to incubate for another 72 h. After 72 h, an MTT cell proliferation assay (Thermo Fisher Scientific, Grand Island, NY) was performed according to the manufacturer's protocol.

2.13. Statistical Analyses. Results were reported as mean \pm standard deviation except where noted. All experiments were replicated at least three times with at least three unique protein batches. Statistical significance was determined with an unequal variance *T*-test. Significance was accepted at $p < 0.05$.

3. RESULTS

3.1. Synthesis and Characterization of Endosomolytic Peptide Fusions. In our previous work, we clustered four EGFR-binding GE11 peptides⁵² onto mCherry protein that was fused to SpyCatcher (SC) to create an EGFR-targeted fluorescent transporter construct capable of cargo attachment through SpyCatcher/SpyTag chemistry⁵³ (4GE11-mCherry-SC).⁴⁶ Briefly, 4GE11-mCherry-SC was generated by a three-step process: (1) four *p*-azido-L-phenylalanine (pAzF) unnatural amino acids (UAAs) were incorporated through amber suppression⁴⁷ onto the N-terminus of mCherry-SC in *E. coli*; (2) an alkyne-GE11 peptide was synthesized with an N-terminal propargylglycine via solid-phase peptide synthesis; and (3) the alkyne-GE11 was reacted to 4pAzF-mCherry-SC through CuAAC (Figure S3A). 4GE11-mCherry-SC demonstrated robust internalization in inflammatory breast cancer (IBC) SUM149 cells compared to that in healthy breast epithelial MCF10A cells, as the MCF10A cells exhibited 5-fold less membrane-associated EGFR as determined by immunos-

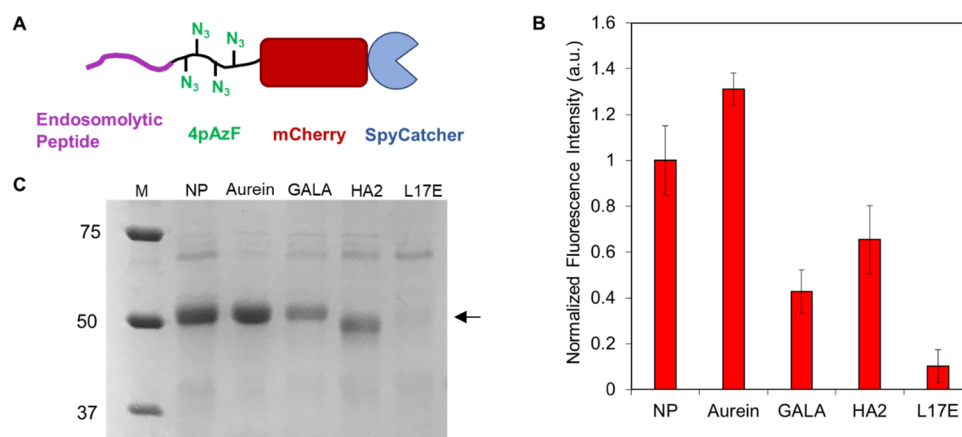


Figure 1. Expression of endosomal peptide fusion proteins. (A) Schematic of endosomal peptide fusions with 4pAzF-mCherry-SC. (B) Soluble lysate mCherry fluorescence normalized to concentration determined by Bradford protein assays. Results were then normalized to expression levels of the original 4pAzF-mCherry-SC protein. Results are shown as mean \pm standard deviation of three independent experiments. (C) SDS-PAGE analysis of His-tag purified constructs. NP (no peptide) denotes the absence of an endosomal escape peptide in the 4pAzF-mCherry-SC protein construct.

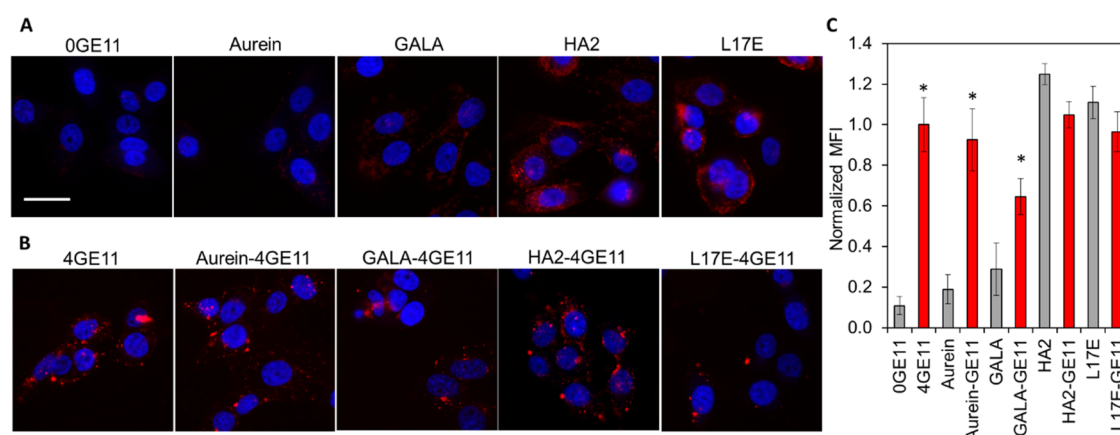


Figure 2. Uptake of protein constructs in IBC SUM149 cells following 3 h incubation. (A) Fluorescence microscopy following treatment with endosomal fusions without GE11 (0GE11). (B) Fluorescence microscopy following treatment with endosomal fusions with four GE11 peptides (4GE11). Cells were stained with DAPI nuclear stain (blue). The scale bar represents 40 μ m. (C) Mean fluorescent intensity of cells treated with endosomal fusions containing 0GE11 (gray) or 4GE11 (red) from flow cytometry analysis. Results are shown as the mean fluorescence intensity \pm standard deviation of data obtained from three independent experiments. *Indicates a statistically significant difference between 0GE11 and 4GE11 conjugates with the same endosomolytic peptide in IBC SUM149 cells ($p < 0.05$).

taining. Additionally, competitive inhibition with EGF in IBC SUM149 cells drastically lowered uptake, demonstrating that the observed internalization was EGFR-mediated. This phenomenon resulted in IBC-specific cell death when a SpyTag (ST)-fused prodrug-converting enzyme was attached to 4GE11-mCherry-SC via SpyCatcher/SpyTag bioconjugation.

Despite successful targeted internalization, 4GE11-mCherry-SC remained entrapped in the endolysosomal pathway leading to lysosomal colocalization (Figure S1A) and rapid lysosomal degradation within 16 h (Figure S1B). To increase the range of cargo that can be delivered with 4GE11-mCherry-SC, an approach to improve the endosomal escape of 4GE11-mCherry-SC was needed. Accordingly, four endosomal escape peptides (Table 1) were genetically fused to the N-terminus of 4pAzF-mCherry-SC and expressed in *E. coli* through amber suppression (Figure 1A). The N-terminus was chosen as the site of modification to ensure the removal of N-terminally truncated proteins containing the active peptides without the fluorescent tag, which could act as competitive inhibitors.

Expression was monitored by measuring the mCherry fluorescence intensity of the clarified protein lysate and normalizing to the fluorescence intensity of 4pAzF-mCherry-SC alone (Figure 1B). The fusions were purified with His-tag Ni-NTA affinity chromatography, and the purified samples were analyzed via SDS-PAGE (Figure 1C). Fusion with Aurein 1.2 resulted in expression levels similar to that of 4pAzF-mCherry-SC alone; however, a moderate decrease in expression was observed when GALA and HA2 were fused to the mCherry construct, with the GALA- and HA2-4pAzF-mCherry-SC expression levels reaching only \sim 50 and 65% of the original 4pAzF-mCherry-SC construct, respectively. Fusion with GALA and HA2 also resulted in a higher level of insoluble protein, which may contribute to the decrease in soluble protein observed (Figure S2). For the L17E fusion, the expression decreased drastically to approximately 15% of the expression level of the original 4pAzF-mCherry-SC, and larger culture volumes were necessary to yield functional quantities.

The four GE11 peptides were conjugated to the pAzF-containing fusions with CuAAC as described in our previous

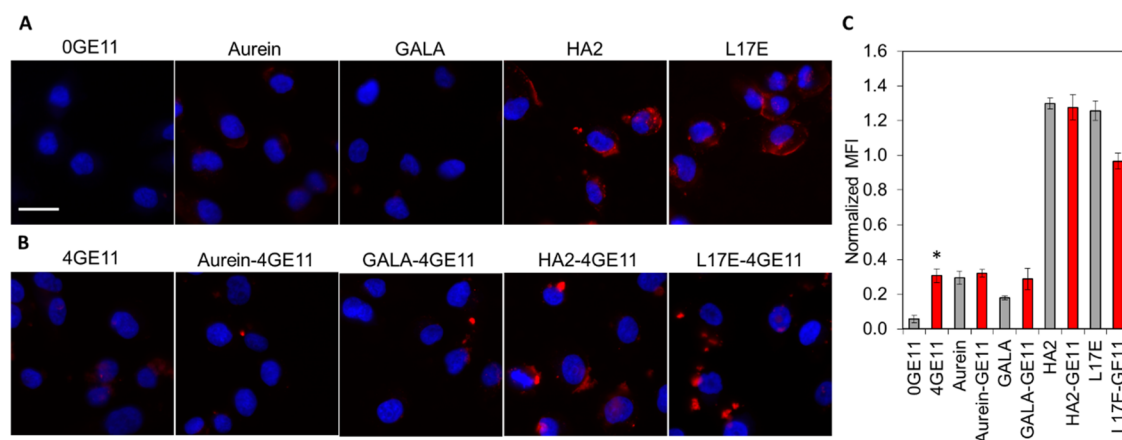


Figure 3. Uptake of protein constructs in MCF10A cells following 3 h incubation. (A) Fluorescence microscopy following treatment with endosomal fusions with 0GE11. (B) Fluorescence microscopy following treatment with endosomal fusions with 4GE11 peptides. Cells were stained with DAPI nuclear stain (blue). Scale bar represents 40 μ m. (C) Mean fluorescent intensity of cells treated with endosomal fusions containing 0GE11 (gray) or 4GE11 (red) from flow cytometry analysis. Results are shown as the mean fluorescence intensity \pm standard deviation of data obtained from three independent experiments. *Indicates a statistically significant difference between 0GE11 and 4GE11 conjugates with the same endosomal peptide in MCF10A cells ($p < 0.05$).

work.⁴⁶ The reaction yield was confirmed by SDS-PAGE analysis (Figure S3). The product band shift following reaction was similar for all constructs, suggesting that pAzF reactivity was not significantly hindered by the presence of the endosomal peptides. Protein fusions without the pAzF residues were also generated to act as 0GE11 controls, and His-tag-purified protein was confirmed by SDS-PAGE (Figure S4).

3.2. Uptake of Endosomal Peptide Fusions in IBC SUM149 Cells. Internalization was initially measured in IBC SUM149 cells expressing high levels of EGFR. Cells were treated with endosomal peptide fusions, and uptake was visualized with fluorescence microscopy for fusions without GE11 peptides (0GE11; Figure 2A) or fusions with four GE11 peptides (4GE11; Figure 2B). Corresponding phase images are provided in the Supplemental Information (Figure S5). Uptake was quantified with flow cytometry (Figure 2C). The mean fluorescence intensity (MFI) of all samples was normalized to the uptake of the original 4GE11-mCherry-SC construct in IBC SUM149 cells without an endosomal peptide. Consistent with our prior studies, EGFR-mediated protein internalization in the absence of endosomal peptides was only observed when 4GE11 peptides were present. The Aurein 1.2 and GALA fusion proteins maintained EGFR specificity, as demonstrated by their significantly higher uptake levels with 4GE11 compared to the same proteins without GE11 peptides (0GE11). The Aurein 1.2 fusions demonstrated the highest fold difference (4.9-fold) between 0GE11- and 4GE11-containing constructs. The fold change was reduced in the GALA-containing constructs to 2.2-fold, but the difference between 0GE11 and 4GE11 remained significant. For fusions with HA2 and L17E, the difference in uptake between the 0GE11 and 4GE11 constructs was not significant, suggesting that an alternative mechanism of internalization was occurring that was not EGFR-specific. It is also worth noting that the cellular localization of 4GE11 fusions appears more punctate inside the cell compared to that of the 0GE11 constructs when internalization is visible. This difference in cellular trafficking could also indicate an alternative uptake mechanism.

3.3. Uptake of Endosomal Peptide Fusions in MCF10A Cells. To further assess the EGFR cell specificity of

the endosomal peptide fusions, mCherry internalization was also assessed in MCF10A breast epithelial cells, which express basal levels of EGFR that are approximately 5 times lower than the EGFR expression levels in IBC SUM149 cells.⁴⁶ MCF10A cells were treated with protein, and uptake was measured. Fluorescence microscopy was used to visualize the internalization of 0GE11 (Figure 3A) and 4GE11 constructs (Figure 3B); corresponding phase images are provided in the Supplemental Information (Figure S6). Flow cytometry was again used to quantify uptake (Figure 3C), and the MFI of all samples was normalized to uptake of the original 4GE11-mCherry-SC construct in IBC SUM149 cells. Low levels of internalization were observed for 0GE11- and 4GE11-mCherry-SC constructs without an endosomal peptide, corroborating our previous work.⁴⁶ The modest increase in uptake with 4GE11 peptides was expected since MCF10A cells express low levels of EGFR. Nonetheless, there was 3-fold higher internalization of 4GE11-mCherry-SC in IBC SUM149 cells as compared to MCF10A cells. Aurein 1.2 and GALA fusions containing 0GE11 demonstrated higher levels of internalization compared to 0GE11 alone, suggesting a minor increase in nonspecific uptake; however, the uptake levels in MCF10A cells were still significantly lower for the 4GE11 fusions compared to targeted uptake levels in IBC SUM149. Specifically, the fold differences between IBC SUM149 cells and MCF10A cells for Aurein 1.2- and GALA-4GE11-mCherry-SC constructs were 2.9-fold and 2.3-fold, respectively, which are comparable to the 3-fold difference observed when no endosomal peptide was fused. Constructs fused with HA2 or L17E demonstrated high levels of internalization in MCF10A whether GE11 peptides were present or not. This once again suggests that the fusion of HA2 or L17E to 4GE11-mCherry-SC promotes internalization through a mechanism other than EGFR-mediated endocytosis, thereby negating cell specificity.

3.4. Endosomal Disruption with Gal8-YFP Assay. We next assessed the bioactivity of each endosomal peptide. Galectin8 (Gal8) visualization was used to measure endosomal disruption in MDA-MB-231 cells stably expressing Gal8-YFP.⁴⁹ Gal8 binds to glycans unique to the inner face of endosomal membranes.⁵⁴ In the event of endosomal

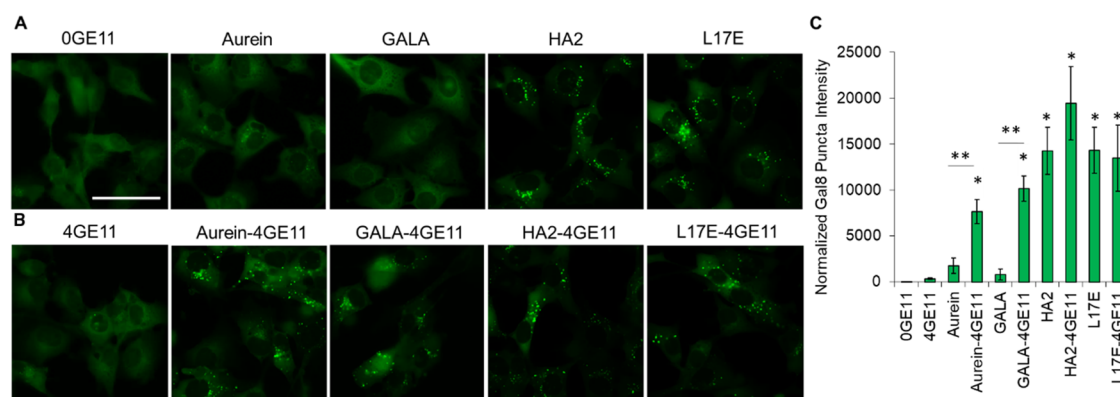


Figure 4. Gal8-YFP endosomal disruption assay. (A) Fluorescence microscopy of Gal8-YFP-expressing MDA-MB-231 cells 16 h following treatment with endosomal fusions without GE11 and (B) endosomal fusions with 4GE11 peptides. Scale bar represents 100 μ m. (C) Gal8-positive puncta intensity normalized to cell count, as determined by MATLAB quantification. Results are shown as the mean \pm standard deviation of data obtained from three independent experiments. * indicates a statistically significant difference in Gal8 puncta intensity compared to that in MDA-MB-231 cells treated with 4GE11-mCherry-SC ($p < 0.05$). ** indicates a statistically significant difference in Gal8 puncta intensity between the same construct with 4GE11 versus 0GE11.

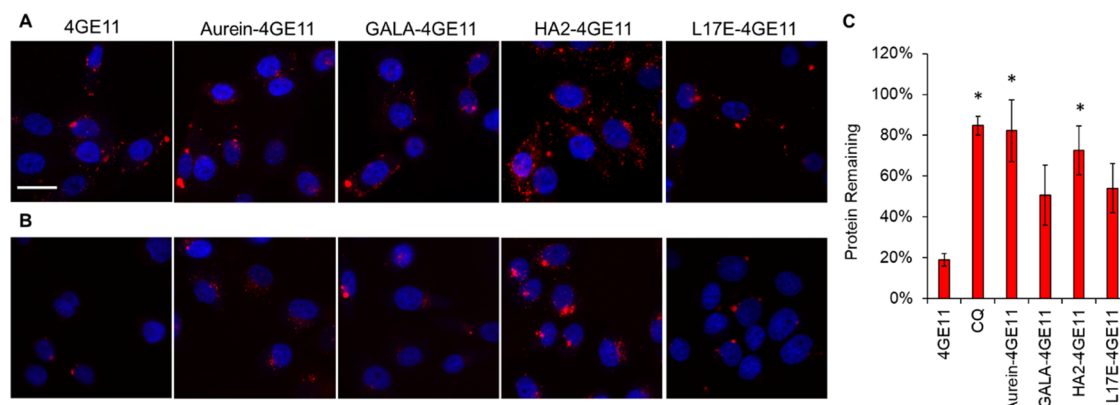


Figure 5. Lysosomal degradation of mCherry in IBC SUM149 cells. Fluorescence microscopy following treatment with endosomal fusions containing 4GE11 at (A) 0 h following protein incubation or (B) 16 h following protein incubation. Cells were stained with DAPI nuclear stain (blue). The scale bar represents 40 μ m. (C) The percent of remaining protein 16 h post incubation compared to 0 h post incubation as determined by flow cytometry. Results are shown as the mean \pm standard deviation of data obtained from three independent experiments. *Indicates a statistically significant difference in protein remaining in IBC SUM149 cells after 16 h compared to cells treated with 4GE11-mCherry-SC ($p < 0.05$).

disruption, Gal8-YFP redistributes from the cytosol into the endosomes, which can be visualized by the appearance of Gal8-positive puncta. MDA-MB-231 cells are triple-negative human epithelial breast cancer cells that overexpress EGFR at levels similar to IBC SUM149 cells.⁵⁵ Previous work has demonstrated the ability of the GE11 peptide to target EGFR overexpression in MDA-MB-231 cells.^{56–59} To confirm internalization, MDA-MB-231 Gal8-YFP cells were treated with 1 μ M of the endosomolytic fusion proteins with 0GE11 or 4GE11 peptides for 3 h and uptake was confirmed by fluorescence microscopy (Figure S7). Uptake levels were similar to those observed in IBC SUM149 cells. Once again, uptake appeared to be EGFR-specific for the Aurein 1.2 and GALA fusions, but the HA2 and L17E fusions were internalized whether 4GE11 was present or not.

Once uptake was confirmed, endosomal disruption was measured in MDA-MB-231 Gal8-YFP cells. Cells were treated with 1 μ M of protein for 3 h to allow internalization, and then, the cells were washed and incubated for an additional 16 h to allow time for endosomal escape. Fluorescence microscopy was used to visualize Gal8-YFP recruitment following treatment

with 0GE11 proteins (Figure 4A) or 4GE11-containing proteins (Figure 4B). Corresponding phase images are provided in the Supplemental Information (Figure S8). For 0GE11 proteins, only HA2 and L17E fusions demonstrated Gal8-YFP recruitment to the endosomes, as demonstrated by the appearance of Gal8-YFP-positive puncta. This result agrees with previous findings, as only the HA2 and L17E fusions were uptaken at high levels without GE11. When cells were treated with 4GE11-containing proteins, Gal8-YFP-positive puncta were visible for all constructs containing endosomolytic peptides, while 4GE11-mCherry-SC alone did not elicit Gal8-YFP redistribution.

To quantify Gal8 recruitment, a MATLAB program, derived from Kilchrist, et al.,⁵⁰ was used to measure the fluorescence intensity of Gal8-YFP-positive puncta normalized to the total number of cells in an image frame (Figures 4C and S9). Minimal endosomal disruption was observed for 0GE11- and 4GE11-mCherry-SC without an endosomolytic peptide fusion partner. Robust endosomal disruption was demonstrated by HA2 and L17E fusions with or without 4GE11, while Aurein 1.2 and GALA fusions demonstrated significantly higher Gal8

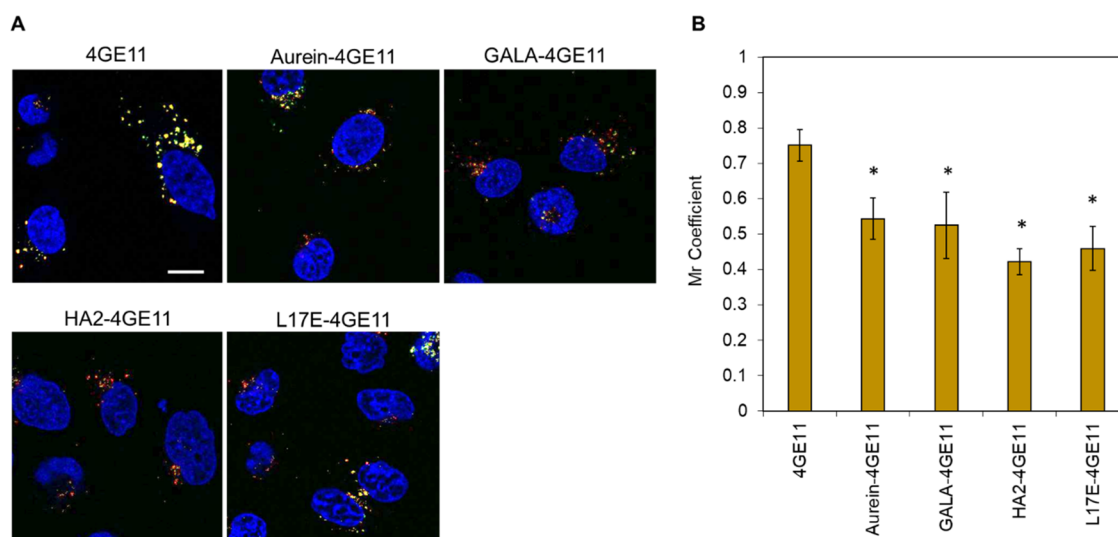


Figure 6. Lysosomal colocalization of protein constructs in IBC SUM149 cells. (A) Fluorescence microscopy following treatment with GE11 endosomal fusions (red) and lysosomal staining (green) with LysoView. The nuclei are stained with DAPI in blue, and colocalization between mCherry and LysoView is represented in yellow. The scale bar represents 10 μ m. (B) Quantification of colocalization between lysosomes and 4GE11-targeted endosomal fusion proteins in IBC SUM149 cells based on the calculation of Mander's coefficients (M_r). A range of 8–12 images were analyzed, approximately 50 cells, per sample, and the M_r was reported as the mean \pm standard deviation. *Indicates a statistically significant difference in lysosomal colocalization compared to 4GE11-mCherry-SC in IBC SUM149 cells ($p < 0.05$).

recruitment when 4GE11 was present compared to 0GE11 constructs. HA2-4GE11-mCherry-SC demonstrated the highest level of endosomal disruption, suggesting superior endosomolytic properties.

3.5. Lysosomal Degradation in IBC SUM149 Cells.

Most proteins trapped within endosomes undergo exocytosis or lysosomal degradation, preventing delivery to the cytosol.⁶⁰ Because of this, only a small amount of 4GE11-mCherry-SC protein was visible inside IBC SUM149 cells at 16 h post internalization (Figure S1A), despite high levels of initial uptake and an intracellular mCherry half-life of 20–30 h.⁶¹ To measure the amount of protein remaining inside IBC SUM149 cells, cells were treated with protein for 3 h before extracellular protein was removed. Immediately after protein treatment (0 h), mCherry internalization was imaged with fluorescence microscopy (Figure 5A). Cells were then incubated for 16 h before fluorescence microscopy was again used to visualize mCherry trafficking (Figure 5B). Corresponding phase images are provided in the Supplemental Information (Figure S10). Sixteen hours was chosen to allow enough time for lysosomal degradation while minimizing dilution from cell proliferation (the doubling time of IBC SUM149 cells is approximately 26 h⁶²). From microscopy, cells treated with endosomolytic peptide fusions contained more mCherry protein at 16 h post internalization as compared to cells treated with 4GE11-mCherry-SC alone. We expected the protein to be diffused throughout the cytosol; however, most of the protein still appeared in bright punctate spots, suggesting endomembrane localization or protein aggregation within the cytosol.

The MFI of cells at 0 and 16 h post internalization was measured with flow cytometry. The percent of protein remaining in the cells after 16 h was quantified by dividing the MFI of cells incubated for 16 h after treatment by the MFI of cells 0 h after treatment (Figures 5C and S12). Less than 20% of protein remained after 16 h in cells treated with 4GE11-mCherry-SC. To demonstrate that this rapid degradation was occurring in the lysosome, cells were treated with

chloroquine (CQ), a weak base that prevents lysosomal acidification and, in turn, inhibits protein degradation by pH-specific enzymes.⁶³ Following CQ treatment, cells were incubated with 4GE11-mCherry-SC and internalized protein was measured at 0 and 16 h post incubation. From fluorescence microscopy, high levels of 4GE11-mCherry-SC remained in cells pretreated with CQ after 16 h (Figure S11). The protein appeared to remain in the endosomal membranes, which agrees with the previous literature showing that higher concentrations or longer treatments of CQ are necessary to rupture the endosomal membrane and promote escape.^{64,65} Here, higher concentrations of CQ led to significant cell toxicity. When cells were pretreated with CQ, nearly 85% of the protein that was internalized remained in the cells after 16 h. This suggests that the rapid disappearance of the 4GE11-mCherry-SC signal is primarily the result of lysosomal degradation. The remaining 15% of protein was likely lost through dilution from cell division or exocytosis. More protein remained after 16 h in cells treated with the endosomolytic peptide fusions compared to cells treated with 4GE11-mCherry-SC alone. Specifically, Aurein 1.2 and HA2 enabled significantly less lysosomal degradation after 16 h, with 82 and 73% of protein remaining, respectively, compared to cells treated with 4GE11 where less than 20% of the originally internalized protein remained. These levels were similar to the outcome after treatment with CQ.

3.6. Lysosomal Colocalization in IBC SUM149 Cells.

The endosomolytic peptide 4GE11-mCherry-SC fusions maintained a punctate distribution characteristic of endomembrane localization 16 h after internalization, despite evidence of endosomal disruption from the Gal8 assay. To assess lysosomal colocalization, IBC SUM149 cells were stained with LysoView, a pH-sensitive dye that localizes in acidic compartments, to visual lysosomal membranes. Cells were treated with protein and incubated for 10 h to allow time for endosomal escape before lysosomes were stained and cells were imaged with confocal microscopy (Figure 6A). To quantify the mCherry

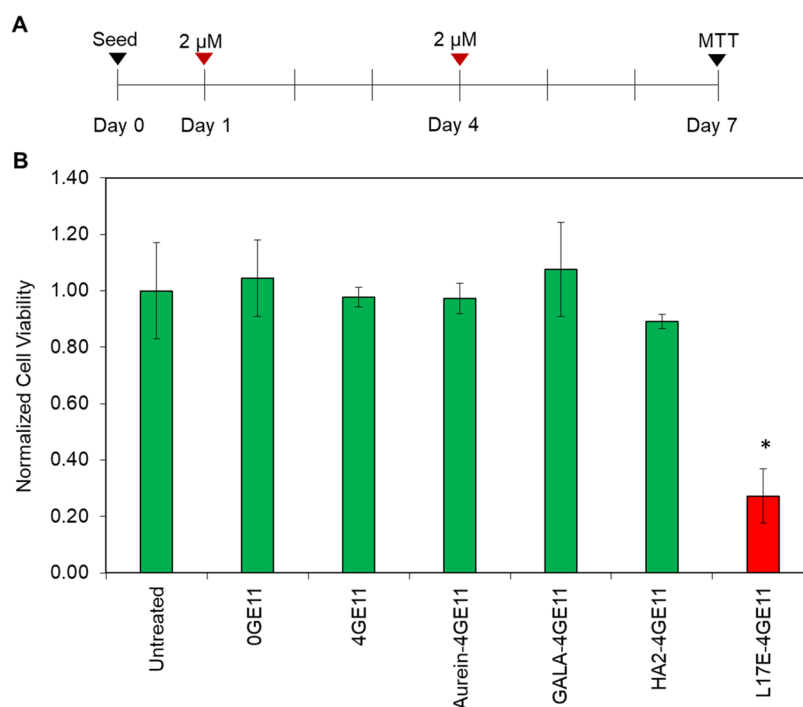


Figure 7. Cell viability assays in IBC SUM149 cells. (A) Cells were treated twice with 2 μ M of endosomolytic 4GE11 proteins. (B) MTT assays were used to assess the viability of IBC SUM149 cells following treatment with endosomolytic peptide fusions. Results are shown as the mean \pm standard deviation of data obtained from three independent experiments. * indicates a statistically significant difference in cell viability compared to IBC SUM149 cells treated with 4GE11-mCherry-SC ($p < 0.05$).

protein (red pixels) colocalized in the lysosomes (green pixels), the Mander's correlation coefficient (M_r) was calculated with Zeiss colocalization software (Figure 6B).⁶⁶ Cells treated with 4GE11-mCherry-SC had the largest M_r value of 0.75, suggesting that 75% of the protein remained entrapped in the lysosome. Endosomolytic peptide fusions all demonstrated significantly lower levels of lysosomal colocalization, with Aurein 1.2, GALA, HA2, and L17E showing 54, 52, 42, and 46% of the internalized protein entrapped in the lysosomes, respectively. HA2 demonstrated the lowest apparent lysosomal colocalization; however, the difference between the four constructs was not significant.

3.7. Cell Viability in IBC SUM149 Cells. Although the lytic properties of endosomolytic peptides are pH-dependent, there is still the potential for reconfiguration and activation at more neutral pH leading to cell membrane lysis. This effect has been documented in the literature for a number of endosomolytic peptides and is believed to be a result of variations in charge distribution and the isoelectric point of the protein fusion.^{67,68} Therefore, we studied the cytotoxicity of each endosomolytic peptide fusion. MTT assays were used to determine the effect of each endosomolytic peptide 4GE11-mCherry-SC fusion on IBC SUM149 cell viability. Cells were treated with 2 μ M of protein twice over 6 days, and the cell viability was measured (Figure 7A). Cell viability of each sample was normalized to the viability of untreated cells (Figure 7B). Aurein 1.2-, GALA-, and HA2-4GE11-mCherry-SC fusions did not exhibit high levels of cytotoxicity (>85% viability) following two treatments; however, cells treated with L17E-4GE11-mCherry-SC were only 25% viable after two treatments, demonstrating that the addition of the L17E peptide significantly hindered IBC SUM149 cell viability.

4. DISCUSSION

Herein, we assessed the bioactivity of four endosomolytic peptides that were genetically fused to an EGFR-targeting fluorescent "transporter" conjugate. We first evaluated recombinant expression yields in *E. coli* when each endosomolytic peptide was fused to the N-terminus of 4pAzF-mCherry-SC. Our results with Aurein 1.2, GALA, and HA2 fusion expression were largely aligned with results from the previous literature,^{36,69–71} with the expression of the Aurein 1.2 fusion partner occurring at similar levels as the base protein constructs. Fusion with GALA and HA2 decreased the expression of the soluble product marginally; however, the yield of soluble protein was still sufficient. To the best of our knowledge, this is the first attempt to genetically fuse L17E directly to a target protein and express the peptide recombinantly, as previous work with L17E peptide has employed solid-phase peptide synthesis.³⁸ The peptide is derived from the antimicrobial peptide m-lycotoxin,⁷³ and while it has been engineered to attenuate lytic activity at neutral pH, recent results have demonstrated that the peptide preferentially perturbs negatively charged membranes, such as the endosomal membrane, without demonstrating pH selectivity.³⁸ Because of this, L17E likely retains its lytic activity toward Gram-negative *E. coli* cells, making recombinant expression an inappropriate method of production.

Endosomolytic peptides have shown some ability to trigger cell internalization, which can hinder targeting specificity. For instance, Aurein 1.2 enhanced the uptake of fused protein nanocarriers in prior work.⁷⁴ Here, fusing a single Aurein 1.2 peptide to 4GE11-mCherry-SC did not significantly increase uptake, indicating that protein internalization remained primarily EGFR-mediated. Despite maintaining some EGFR specificity, GALA decreased the internalization of 4GE11-

mCherry-SC in IBC SUM149 cells. Interestingly, this phenomenon has been observed in the literature before with other GALA fusion proteins; GALA's hydrophobicity has been hypothesized to trigger peptide aggregation on the cell membrane, blocking further cytoplasmic transport.^{68,75} This effect may be a driver of the behavior we observed, particularly considering the increase in insoluble protein expression that was evident for GALA-4pAzF-mCherry-SC. Alternatively, the high net negative charge of the peptide at neutral pH could be hindering interaction with the negatively charged cell membrane lipid bilayer.⁷⁶ Here, HA2 and L17E did not maintain EGFR specificity of 4GE11-mCherry-SC, suggesting an alternative mechanism of internalization. Recent literature demonstrated that the HA2 fusion to the N-terminus of ligand-targeted protein nanoparticles drastically reduced cell receptor specificity, in agreement with our findings.⁶⁷ Likewise, previous work demonstrated that the L17E peptide was rapidly internalized through micropinocytosis and membrane ruffling due to its positive net charge.^{38,77} These phenomena likely explain the alternative uptake mechanism observed here. These behaviors highlight the limitations of HA2 and L17E modifications when receptor targeting is desired. We expected higher internalization with the endosomolytic fusions containing 4GE11, especially with L17E and HA2, which showed high internalization with GE11 peptides. The results appear to suggest that the mechanisms of internalization are not additive. The GE11 peptides are buried further into the protein sequence than the endosomolytic peptides, which are directly on the N-terminus. One possibility is that the cell preferentially binds HA2 or L17E before the GE11 peptides can engage the receptor. Further studies varying the location of the GE11 peptides could test this hypothesis.

The bioactivity of each endosomolytic peptide was assessed by evaluating endosomal disruption, lysosomal degradation, and lysosomal colocalization. The Gal8 assay demonstrated increased levels of endosomal disruption when endosomolytic peptides were fused to 4GE11-mCherry-SC, with HA2 showing the highest levels of disruption. We had expected the carpet-like peptides to show the highest levels of endosomal disruption because they are believed to form larger pores in the membrane; however, it is possible that fusing these peptides to proteins hinders their membrane-disruption activity more than pore-forming peptides. This possibility is further supported by the higher levels of endosomal disruption caused by GALA as compared to Aurein 1.2, despite lower levels of internalization. L17E also showed lower levels of endosomal disruption compared to HA2 despite similar levels of internalization. This could possibly be explained by recent results, which suggest that the major mechanism of L17E internalization is a membrane ruffling effect, leading to direct cytosolic uptake rather than cytosolic delivery through endosomal escape.⁷⁷ Directly fusing L17E to the cargo protein may, however, affect the internalization mechanism since roughly half of the internalized protein was in the lysosomes from our lysosomal colocalization study. Additionally, we delivered significantly less L17E peptides than the original study, and the delivery concentration of cationic peptides has been shown to affect the mechanism of internalization. Direct cell membrane penetration is more likely at higher concentrations.⁷⁸

For all endosomolytic peptide fusions, roughly half of the protein remained trapped in the lysosomes, likely explaining the mCherry puncta observed after 16 h. Higher peptide

concentrations would likely enhance the endosomal escape, but depending on the cargo potency, the level of escape we obtained may be sufficient to elicit a therapeutic response. For example, similar M_r values from lysosomal colocalization studies have resulted in the efficient cytosolic delivery of siRNA for gene knockdown.⁴⁹ The visible puncta after 16 h could also be an effect of protein entrapped in the lysosome despite endosomal lysis. In previous studies, endosomolytic peptides have successfully induced endosomal lysis while remaining trapped inside endosomes.^{72,79} Employing a mechanism for releasing the cargo, such as a cleavable linker or disulfide bonds, may be necessary to improve cytosolic delivery. Likewise, taking advantage of a protein that naturally binds cargo at neutral pH but releases it at acidic pH could be advantageous. For example, the p19 protein, derived from tombusviruses, has been shown to bind siRNA at neutral pH and release siRNA in acidic environments, e.g., within the endosome.^{80,81}

Our results demonstrate that Aurein 1.2-, GALA-, and HA2-fused 4GE11-mCherry-SC were not cytotoxic at high concentrations. This agrees with previous work wherein cells treated with Aurein 1.2, GALA, and HA2 fusion proteins did not show high levels of toxicity.^{69,82,83} L17E fused to 4GE11-mCherry-SC, on the other hand, demonstrated significant toxicity toward IBC SUM149 cells, which has not been previously reported. The original work codelivered the L17E peptide with therapeutic protein cargos rather than fusing the peptide directly to the cargo, as done here.³⁸

The results found here do not indicate that one mechanism of endosomal disruption outcompetes another, but further studies are necessary with a larger library of peptides to confirm this result. The endosomolytic peptides appeared to elicit high levels of endosomal disruption regardless of the mechanism. This resulted in decreased lysosomal degradation, likely by preventing endolysosomal acidification needed for hydrolytic enzyme activity. Despite this, a large portion of the protein remained in the lysosome, suggesting that lysis is not enough to elicit high levels of endosomal escape, possibly due to the protein remaining fused to the endosomal membrane. Future studies comparing cytosolic delivery of an active cargo that can be released from the delivery vehicle may highlight larger activity differences between each peptide.

5. CONCLUSIONS

Herein, we assessed the bioactivity of four endosomolytic peptides fused to an EGFR-targeting protein conjugate capable of serving as a transporter for therapeutic proteins. All endosomolytic peptides provided substantial endosomal disruption and lower levels of lysosomal degradation, with HA2 exhibiting the most potent membrane activity. Lysosomal colocalization studies also demonstrated significantly lower levels of lysosomal colocalization in constructs fused to endosomolytic peptides; however, even with the peptide fusions, approximately half of the protein remained entrapped in endosomes, highlighting the potential importance of employing a cargo release mechanism to separate the active drug from a delivery module fused to the endosomal membrane. Aurein 1.2 and GALA retained EGFR specificity, while HA2 and L17E enhanced cell penetration independent of EGFR expression, limiting their use when cell specificity is desired. Finally, L17E expressed poorly as a fusion partner and led to high levels of cytotoxicity, demonstrating that direct fusion is an inappropriate strategy for its use. Overall, Aurein

1.2 fused to our EGFR-targeting conjugate exhibited the best balance of endosomolytic capacity and high EGFR specificity. These results lay the groundwork for delivering a variety of therapeutic cargos to intracellular compartments using our EGFR-targeted conjugate. Moreover, the results reported here demonstrate the ability of a single genetically fused endosomolytic peptide to drastically change the bioactivity, cytotoxicity, and targeting specificity of a protein delivery system. This highlights the importance of holistic evaluations of endosomolytic activity and cell uptake when designing protein delivery systems and reveals the need for further studies assessing the effect these peptides have on the delivery of proteins that vary in size and composition.

■ ASSOCIATED CONTENT

Supporting Information

The Supporting Information is available free of charge at <https://pubs.acs.org/doi/10.1021/acs.molpharmaceut.1c00788>.

4GE11-mCherry-SC endosomal entrapment; expression of endosomolytic peptide fusions; GE11 conjugation of endosomolytic peptide fusions; expression of endosomolytic peptide fusions without UAA incorporation; phase images for IBC SUM149 internalization studies; phase images for MCF10A internalization studies; uptake of endosomolytic peptide fusions in MDA-MB-231 cells; phase images for the MDA-MB-231 Gal8 assay; example of Gal8 intensity quantification from the MATLAB code; phase images for lysosomal degradation studies; fluorescence microscopy of 4GE11-mCherry-SC following CQ treatment; flow cytometry histograms for the lysosomal degradation studies; and DNA oligos and nucleotide sequences used in this study (PDF)

■ AUTHOR INFORMATION

Corresponding Authors

Wilfred Chen – Department of Chemical and Biomolecular Engineering, University of Delaware, Newark, Delaware 19716, United States; orcid.org/0000-0002-6386-6958; Email: wilfred@udel.edu

Millicent O. Sullivan – Department of Chemical and Biomolecular Engineering, University of Delaware, Newark, Delaware 19716, United States; Email: rmlieser@udel.edu

Authors

Rachel M. Lieser – Department of Chemical and Biomolecular Engineering, University of Delaware, Newark, Delaware 19716, United States; orcid.org/0000-0002-7597-0672

Qirun Li – Department of Chemical and Biomolecular Engineering, University of Delaware, Newark, Delaware 19716, United States

Complete contact information is available at:

<https://pubs.acs.org/doi/10.1021/acs.molpharmaceut.1c00788>

Notes

The authors declare no competing financial interest.

■ ACKNOWLEDGMENTS

R.M.L. was supported by grants from the National Science Foundation (1510817 and 1144726). The authors thank Dr. Sylvain Le Marchand at the Bio-Imaging Center at the

Delaware Biotechnology Institute for assistance with confocal microscopy. The authors thank NIH-NIGMS (P20 GM103445), the NSF (IIA-1301765), and the State of Delaware for support for confocal microscope access. Any opinions, findings, and conclusions or recommendations expressed in this material are those of the authors and do not necessarily reflect the view of the National Science Foundation.

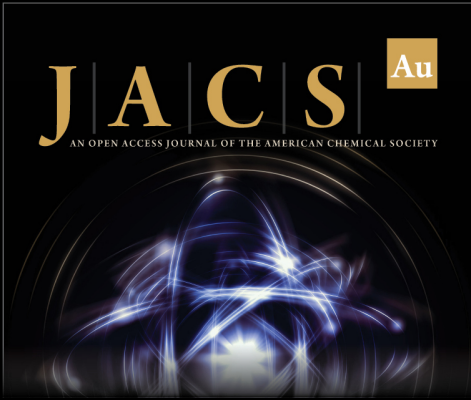
■ REFERENCES

- (1) Fu, A. L.; Tang, R.; Hardie, J.; Farkas, M. E.; Rotello, V. M. Promises and Pitfalls of Intracellular Delivery of Proteins. *Bioconjugate Chem.* **2014**, *25*, 1602–1608.
- (2) Lau, J. L.; Dunn, M. K. Therapeutic peptides: Historical perspectives, current development trends, and future directions. *Bioorg. Med. Chem.* **2018**, *26*, 2700–2707.
- (3) Dang, C. V.; Reddy, E. P.; Shokat, K. M.; Soucek, L. Drugging the 'undruggable' cancer targets. *Nat. Rev. Cancer* **2017**, *17*, 502–508.
- (4) Gaynor, A. S.; Chen, W. Induced prodrug activation by conditional protein degradation. *J. Biotechnol.* **2017**, *260*, 62–66.
- (5) Ren, D. M.; Dalmau, M.; Randall, A.; Shindel, M. M.; Baldi, P.; Wang, S. W. Biomimetic Design of Protein Nanomaterials for Hydrophobic Molecular Transport. *Adv. Funct. Mater.* **2012**, *22*, 3170–3180.
- (6) Bellini, M.; Mazzucchelli, S.; Galbiati, E.; Sommaruga, S.; Fiandra, L.; Truffi, M.; Rizzuto, M. A.; Colombo, M.; Tortora, P.; Corsi, F.; Prosperi, D. Protein nanocages for self-triggered nuclear delivery of DNA-targeted chemotherapeutics in Cancer Cells. *J. Controlled Release* **2014**, *196*, 184–196.
- (7) Danielson, D. C.; Pezacki, J. P. Studying the RNA silencing pathway with the p19 protein. *FEBS Lett.* **2013**, *587*, 1198–1205.
- (8) Choi, K. M.; Kim, K.; Kwon, I. C.; Kim, I. S.; Ahn, H. J. Systemic Delivery of siRNA by Chimeric Capsid Protein: Tumor Targeting and RNAi Activity in Vivo. *Mol. Pharmaceutics* **2013**, *10*, 18–25.
- (9) Chen, L. S.; Wang, M.; Ou, W. C.; Fung, C. Y.; Chen, P. L.; Chang, C. F.; Huang, W. S.; Wang, J. Y.; Lin, P. Y.; Chang, D. Efficient gene transfer using the human JC virus-like particle that inhibits human colon adenocarcinoma growth in a nude mouse model. *Gene Ther.* **2010**, *17*, 1033–1041.
- (10) Fang, C. Y.; Lin, P. Y.; Ou, W. C.; Chen, P. L.; Shen, C. H.; Chang, D. C.; Wang, M. L. Analysis of the size of DNA packaged by the human JC virus-like particle. *J. Virol. Methods* **2012**, *182*, 87–92.
- (11) Ruben, S.; Perkins, A.; Purcell, R.; Joung, K.; Sia, R.; Burghoff, R.; Haseltine, W. A.; Rosen, C. A. Structural and functional characterization of human immunodeficiency virus TAT protein. *J. Virol.* **1989**, *63*, 1–8.
- (12) Guelen, L.; Paterson, H.; Gaken, J.; Meyers, M.; Farzaneh, F.; Tavassoli, M. TAT-apoptin is efficiently delivered and induces apoptosis in cancer cells. *Oncogene* **2004**, *23*, 1153–1165.
- (13) Fawell, S.; Seery, J.; Daikh, Y.; Moore, C.; Chen, L. L.; Pepinsky, B.; Barsoum, J. TAT-mediated delivery of heterologous proteins into cells. *Proc. Natl. Acad. Sci. U.S.A.* **1994**, *91*, 664–668.
- (14) Kaplan, I. M.; Wadia, J. S.; Dowdy, S. F. Cationic TAT peptide transduction domain enters cells by macropinocytosis (vol 102, pg 247, 2005). *J. Controlled Release* **2005**, *107*, 571–572.
- (15) Richard, J. P.; Melikov, K.; Brooks, H.; Prevot, P.; Lebleu, B.; Chernomordik, L. V. Cellular uptake of unconjugated TAT peptide involves clathrin-dependent endocytosis and heparan sulfate receptors. *J. Biol. Chem.* **2005**, *280*, 15300–15306.
- (16) Wadia, J. S.; Stan, R. V.; Dowdy, S. F. Transducible TAT-HA fusogenic peptide enhances escape of TAT-fusion proteins after lipid raft macropinocytosis. *Nat. Med.* **2004**, *10*, 310–315.
- (17) Potocky, T. B.; Menon, A. K.; Gellman, S. H. Cytoplasmic and nuclear delivery of a TAT-derived peptide and a beta-peptide after endocytic uptake into HeLa cells. *J. Biol. Chem.* **2003**, *278*, 50188–50194.
- (18) Falnes, P. O.; Wesche, J.; Olsnes, S. Ability of the Tat basic domain and VP22 to mediate cell binding, but not membrane

translocation of the diphtheria toxin A-fragment. *Biochemistry* **2001**, *40*, 4349–4358.

- (19) Salerno, J. C.; Ngwa, V. M.; Nowak, S. J.; Chrestensen, C. A.; Healey, A. N.; McMurry, J. L. Novel cell-penetrating peptide-adaptors effect intracellular delivery and endosomal escape of protein cargos (vol 129, pg 893, 2016). *J. Cell Sci.* **2016**, *129*, 2473–2474.
- (20) Pennarun, B.; Gaidos, G.; Bucur, O.; Tinari, A.; Rupasinghe, C.; Jin, T.; Dewar, R.; Song, K.; Santos, M. T.; Malorni, W.; Mierke, D.; Khosravi-Far, R. killerFLIP: a novel lytic peptide specifically inducing cancer cell death. *Cell Death Dis.* **2013**, *4*, No. e894.
- (21) Lincoff, A. M.; Roe, M.; Aylward, P.; Galla, J.; Rynkiewicz, A.; Guetta, V.; Zelizko, M.; Kleiman, N.; White, H.; McErlean, E.; Erlinge, D.; Laine, M.; Ferreira, J. M. D.; Goodman, S.; Mehta, S.; Atar, D.; Suryapranata, H.; Jensen, S. E.; Forster, T.; Fernandez-Ortiz, A.; Schoors, D.; Radke, P.; Belli, G.; Brennan, D.; Bell, G.; Krucoff, M. Inhibition of delta-protein kinase C by delcasertib as an adjunct to primary percutaneous coronary intervention for acute anterior ST-segment elevation myocardial infarction: results of the PROTECTION AMI Randomized Controlled Trial. *Eur. Heart J.* **2014**, *35*, 2516–U171.
- (22) Varkouhi, A. K.; Scholte, M.; Storm, G.; Haisma, H. J. Endosomal escape pathways for delivery of biologicals. *J. Controlled Release* **2011**, *151*, 220–228.
- (23) Mudhakir, D.; Harashima, H. Learning from the Viral Journey: How to Enter Cells and How to Overcome Intracellular Barriers to Reach the Nucleus. *AAPS J.* **2009**, *11*, No. 65.
- (24) Futaki, S. Design and Creation of Functional Membrane-Interacting Peptides. *J. Synth. Org. Chem., Jpn.* **2020**, *78*, 1058–1065.
- (25) Ehrenstein, G.; Lecar, H. Electrically gated ionic channels in lipid bilayers. *Q. Rev. Biophys.* **1977**, *10*, 1–34.
- (26) Brabec, M.; Schober, D.; Wagner, E.; Bayer, N.; Murphy, R. F.; Blaas, D.; Fuchs, R. Opening of size-selective pores in endosomes during human rhinovirus serotype 2 in vivo uncoating monitored by single-organelle flow analysis. *J. Virol.* **2005**, *79*, 1008–1016.
- (27) Nir, S.; Nieva, J. L. Interactions of peptides with liposomes: pore formation and fusion. *Prog. Lipid Res.* **2000**, *39*, 181–206.
- (28) Galloux, M.; Libersou, S.; Morellet, N.; Bouaziz, S.; Da Costa, B.; Ouldali, M.; Lepault, J.; Delmas, B. Infectious bursal disease virus, a non-enveloped virus, possesses a capsid-associated peptide that deforms and perforates biological membranes. *J. Biol. Chem.* **2007**, *282*, 20774–20784.
- (29) Li, W. J.; Nicol, F.; Szoka, F. C. GALA: a designed synthetic pH-responsive amphipathic peptide with applications in drug and gene delivery. *Adv. Drug Delivery Rev.* **2004**, *56*, 967–985.
- (30) Cross, K. J.; Langley, W. A.; Russell, R. J.; Skehel, J. J.; Steinhauer, D. A. Composition and Functions of the Influenza Fusion Peptide. *Protein Pept. Lett.* **2009**, *16*, 766–778.
- (31) Kwon, E. J.; Bergen, J. M.; Pun, S. H. Application of an HIV gp41-derived peptide for enhanced intracellular trafficking of synthetic gene and siRNA delivery vehicles. *Bioconjugate Chem.* **2008**, *19*, 920–927.
- (32) Srinivas, S. K.; Srinivas, R. V.; Anantharamaiah, G. M.; Segrest, J. P.; Compans, R. W. Membrane interactions of synthetic peptides corresponding to amphipathic helical segments of the human-immunodeficiency-virus type-1 envelope glycoprotein. *J. Biol. Chem.* **1992**, *267*, 7121–7127.
- (33) Pouny, Y.; Rapaport, D.; Mor, A.; Nicolas, P.; Shai, Y. Interaction of antimicrobial dermaseptin and its fluorescently labeled analogs with phospholipid-membranes. *Biochemistry* **1992**, *31*, 12416–12423.
- (34) Hinz, A.; Galla, H. J. Viral membrane penetration: lytic activity of a nodavirus fusion peptide. *Eur. Biophys. J.* **2005**, *34*, 285–293.
- (35) Oren, Z.; Shai, Y. Mode of action of linear amphipathic alpha-helical antimicrobial peptides. *Biopolymers* **1998**, *47*, 451–463.
- (36) Li, M.; Tao, Y.; Shu, Y. L.; LaRochelle, J. R.; Steinauer, A.; Thompson, D.; Schepartz, A.; Chen, Z. Y.; Liu, D. R. Discovery and Characterization of a Peptide That Enhances Endosomal Escape of Delivered Proteins in Vitro and in Vivo. *J. Am. Chem. Soc.* **2015**, *137*, 14084–14093.
- (37) Shahmiri, M.; Cornell, B.; Mechler, A. Phenylalanine residues act as membrane anchors in the antimicrobial action of Aurein 1.2. *Biointerphases* **2017**, *12*, No. 05G605.
- (38) Akishiba, M.; Takeuchi, T.; Kawaguchi, Y.; Sakamoto, K.; Yu, H. H.; Nakase, I.; Takatani-Nakase, T.; Madani, F.; Graslund, A.; Futaki, S. Cytosolic antibody delivery by lipid-sensitive endosomolytic peptide. *Nat. Chem.* **2017**, *9*, 751–761.
- (39) Lee, H.; Jeong, J. H.; Park, T. G. A new gene delivery formulation of polyethylenimine/DNA complexes coated with PEG conjugated fusogenic peptide. *J. Controlled Release* **2001**, *76*, 183–192.
- (40) Hatakeyama, H.; Ito, E.; Akita, H.; Oishi, M.; Nagasaki, Y.; Futaki, S.; Harashima, H. A pH-sensitive fusogenic peptide facilitates endosomal escape and greatly enhances the gene silencing of siRNA-containing nanoparticles in vitro and in vivo. *J. Controlled Release* **2009**, *139*, 127–132.
- (41) Kwon, E. J.; Liong, S.; Pun, S. H. A Truncated HGP Peptide Sequence That Retains Endosomolytic Activity and Improves Gene Delivery Efficiencies. *Mol. Pharmaceutics* **2010**, *7*, 1260–1265.
- (42) Sala, R.; Sanchez-Garcia, L.; Serna, N.; Cespedes, M. V.; Casanova, I.; Roldan, M.; Sanchez-Chardi, A.; Unzueta, U.; Vazquez, E.; Manguera, R.; Villaverde, A. Collaborative membrane activity and receptor-dependent tumor cell targeting for precise nanoparticle delivery in CXCR4(+) colorectal cancer. *Acta Biomater.* **2019**, *99*, 426–432.
- (43) Lou, B.; De Koker, S.; Lau, C. Y. J.; Hennink, W. E.; Mastrobattista, E. mRNA Polyplexes with Post-Conjugated GALA Peptides Efficiently Target, Transfect, and Activate Antigen Presenting Cells. *Bioconjugate Chem.* **2019**, *30*, 461–475.
- (44) Lam, P.; Steinmetz, N. F. Delivery of siRNA therapeutics using cowpea chlorotic mottle virus-like particles. *Biomater. Sci.* **2019**, *7*, 3138–3142.
- (45) Sudo, K.; Niikura, K.; Iwaki, K.; Kohyama, S.; Fujiwara, K.; Doi, N. Human-derived fusogenic peptides for the intracellular delivery of proteins. *J. Controlled Release* **2017**, *255*, 1–11.
- (46) Lieser, R. M.; Chen, W.; Sullivan, M. O. Controlled Epidermal Growth Factor Receptor Ligand Display on Cancer Suicide Enzymes via Unnatural Amino Acid Engineering for Enhanced Intracellular Delivery in Breast Cancer Cells. *Bioconjugate Chem.* **2019**, *30*, 432–442.
- (47) Chatterjee, A.; Sun, S. B.; Furman, J. L.; Xiao, H.; Schultz, P. G. A Versatile Platform for Single- and Multiple-Unnatural Amino Acid Mutagenesis in *Escherichia coli*. *Biochemistry* **2013**, *52*, 1828–1837.
- (48) Van den Eynden, G.; Van Laere, S.; Van der Auwera, I.; Merajver, S.; Van Marck, E.; van Dam, P.; Vermeulen, P.; Dirix, L.; van Golen, K. Overexpression of caveolin-1 and -2 in cell lines and in human samples of inflammatory breast cancer. *Breast Cancer Res. Treat.* **2006**, *95*, 219–228.
- (49) Kilchrist, K. V.; Dimobi, S. C.; Jackson, M. A.; Evans, B. C.; Werfel, T. A.; Dailing, E. A.; Bedingfield, S. K.; Kelly, I. B.; Duvall, C. L. Gal8 Visualization of Endosome Disruption Predicts Carrier-Mediated Biologic Drug Intracellular Bioavailability. *ACS Nano* **2019**, *13*, 1136–1152.
- (50) Kilchrist, K. V. *Galectin 8 Recruitment Analysis MATLAB Software*; figshare, 2018.
- (51) Li, Q. *Galectin 8 Recruitment Quantification*; figshare, 2021.
- (52) Li, Z. H.; Zhao, R. J.; Wu, X. H.; Sun, Y.; Yao, M.; Li, J. J.; Xu, Y. H.; Gu, J. R. Identification and characterization of a novel peptide ligand of epidermal growth factor receptor for targeted delivery of therapeutics. *FASEB J.* **2005**, *19*, 1978–1985.
- (53) Zakeri, B.; Fierer, J. O.; Celik, E.; Chittock, E. C.; Schwarz-Linek, U.; Moy, V. T.; Howarth, M. Peptide tag forming a rapid covalent bond to a protein, through engineering a bacterial adhesin. *Proc. Natl. Acad. Sci. U.S.A.* **2012**, *109*, E690–E697.
- (54) Thurston, T. L. M.; Wandel, M. P.; von Muhlen, N.; Foeglein, A.; Randow, F. Galectin 8 targets damaged vesicles for autophagy to defend cells against bacterial invasion. *Nature* **2012**, *482*, 414–U1515.

- (55) Lev, D. C.; Kim, L. S.; Melnikova, V.; Ruiz, M.; Ananthaswamy, H. N.; Price, J. E. Dual blockade of EGFR and ERK1/2 phosphorylation potentiates growth inhibition of breast cancer cells. *Br. J. Cancer* **2004**, *91*, 795–802.
- (56) Hu, D. R.; Mezghrani, O.; Zhang, L.; Chen, Y.; Ke, X.; Ci, T. Y. GE11 peptide modified and reduction-responsive hyaluronic acid-based nanoparticles induced higher efficacy of doxorubicin for breast carcinoma therapy. *Int. J. Nanomed.* **2016**, *11*, 5125–5147.
- (57) Müller, K.; Klein, P. M.; Heissig, P.; Roidl, A.; Wagner, E. EGF receptor targeted lipo-oligocation polyplexes for antitumoral siRNA and miRNA delivery. *Nanotechnology* **2016**, *27*, No. 464001.
- (58) Abyaneh, H. S.; Soleimani, A. H.; Vakili, M. R.; Soudy, R.; Kaur, K.; Cuda, F.; Tavassoli, A.; Lavasanifar, A. Modulation of Hypoxia-Induced Chemoresistance to Polymeric Micellar Cisplatin: The Effect of Ligand Modification of Micellar Carrier Versus Inhibition of the Mediators of Drug Resistance. *Pharmaceutics* **2018**, *10*, No. 196.
- (59) Hossein-Nejad-Ariani, H.; Althagafi, E.; Kaur, K. Small Peptide Ligands for Targeting EGFR in Triple Negative Breast Cancer Cells. *Sci. Rep.* **2019**, *9*, No. 2723.
- (60) Munsell, E. V.; Ross, N. L.; Sullivan, M. O. Journey to the Center of the Cell: Current Nanocarrier Design Strategies Targeting Biopharmaceuticals to the Cytoplasm and Nucleus. *Curr. Pharm. Des.* **2016**, *22*, 1227–1244.
- (61) Subach, F. V.; Piatkevich, K. D.; Verkhusa, V. V. Directed molecular evolution to design advanced red fluorescent proteins. *Nat. Methods* **2011**, *8*, 1019–1026.
- (62) Tesauro, C.; Simonsen, A. K.; Andersen, M. B.; Petersen, K. W.; Kristoffersen, E. L.; Algreen, L.; Hansen, N. Y.; Andersen, A. B.; Jakobsen, A. K.; Stougaard, M.; Gromov, P.; Knudsen, B. R.; Gromova, I. Topoisomerase I activity and sensitivity to camptothecin in breast cancer-derived cells: a comparative study. *BMC Cancer* **2019**, *19*, No. 1158.
- (63) Baradaran Eftekhari, R.; Maghsoudnia, N.; Dorkoosh, F. A. Chloroquine: a brand-new scenario for an old drug. *Expert Opin. Drug Delivery* **2020**, *17*, 275–277.
- (64) Mellert, K.; Lamla, M.; Scheffzek, K.; Wittig, R.; Kaufmann, D. Enhancing Endosomal Escape of Transduced Proteins by Photochemical Internalisation. *PLoS One* **2012**, *7*, No. e52473.
- (65) Cervia, L. D.; Chang, C. C.; Wang, L. L.; Yuan, F. Distinct effects of endosomal escape and inhibition of endosomal trafficking on gene delivery via electroporation. *PLoS One* **2017**, *12*, No. e0171699.
- (66) Manders, E. M. M.; Verbeek, F. J.; Aten, J. A. Measurement of colocalization of objects in dual-color confocal images. *J. Microsc.* **1993**, *169*, 375–382.
- (67) Sánchez-García, L.; Serna, N.; Mattanovich, M.; Cazzanelli, P.; Sanchez-Chardi, A.; Conchillo-Sole, O.; Cortes, F.; Daura, X.; Unzueta, U.; Mangués, R.; Villaverde, A.; Vázquez, E. The fusogenic peptide HA2 impairs selectivity of CXCR4-targeted protein nanoparticles. *Chem. Commun.* **2017**, *53*, 4565–4568.
- (68) Li, C.; Cao, X. W.; Zhao, J.; Wang, F. J. Effective Therapeutic Drug Delivery by GALA3, an Endosomal Escape Peptide with Reduced Hydrophobicity. *J. Membr. Biol.* **2020**, *253*, 139–152.
- (69) Lim, S. I.; Lukianov, C. I.; Champion, J. A. Self-assembled protein nanocarrier for intracellular delivery of antibody. *J. Controlled Release* **2017**, *249*, 1–10.
- (70) Li, Y. F. Carrier proteins for fusion expression of antimicrobial peptides in *Escherichia coli*. *Biotechnol. Appl. Biochem.* **2009**, *54*, 1–9.
- (71) Li, Y. F. Recombinant production of antimicrobial peptides in *Escherichia coli*: A review. *Protein Expression Purif.* **2011**, *80*, 260–267.
- (72) Lee, Y. J.; Johnson, G.; Peltier, G. C.; Pellois, J. P. A HA2-Fusion tag limits the endosomal release of its protein cargo despite causing endosomal lysis. *Biochim. Biophys. Acta, Gen. Subj.* **2011**, *1810*, 752–758.
- (73) Yan, L.; Adams, M. E. Lycotoxins, antimicrobial peptides from venom of the wolf spider *Lycosa carolinensis*. *J. Biol. Chem.* **1998**, *273*, 2059–2066.
- (74) Berckman, E. A.; Chen, W. Self-assembling protein nanocages for modular enzyme assembly by orthogonal bioconjugation. *Biotechnol. Prog.* **2021**, No. e3190.
- (75) Calamai, M.; Taddei, N.; Stefani, M.; Ramponi, G.; Chiti, F. Relative influence of hydrophobicity and net charge in the aggregation of two homologous proteins. *Biochemistry* **2003**, *42*, 15078–15083.
- (76) Fröhlich, E. The role of surface charge in cellular uptake and cytotoxicity of medical nanoparticles. *Int. J. Nanomed.* **2012**, *7*, 5577–5591.
- (77) Akishiba, M.; Futaki, S. Inducible Membrane Permeabilization by Attenuated Lytic Peptides: A New Concept for Accessing Cell Interiors through Ruffled Membranes. *Mol. Pharmaceutics* **2019**, *16*, 2540–2548.
- (78) Futaki, S.; Arafles, J. V. V.; Hirose, H. Peptide-assisted Intracellular Delivery of Biomacromolecules. *Chem. Lett.* **2020**, *49*, 1088–1094.
- (79) Lee, Y. J.; Johnson, G.; Pellois, J. P. Modeling of the Endosomolytic Activity of HA2-TAT Peptides with Red Blood Cells and Ghosts. *Biochemistry* **2010**, *49*, 7854–7866.
- (80) Vargason, J. M.; Szitty, G.; Burgan, J.; Hall, T. M. T. Size selective recognition of siRNA by an RNA silencing suppressor. *Cell* **2003**, *115*, 799–811.
- (81) Choi, K. M.; Choi, S. H.; Jeon, H.; Kim, I. S.; Ahn, H. J. Chimeric Capsid Protein as a Nanocarrier for siRNA Delivery: Stability and Cellular Uptake of Encapsulated siRNA. *ACS Nano* **2011**, *5*, 8690–8699.
- (82) Liou, J. S.; Liu, B. R.; Martin, A. L.; Huang, Y. W.; Chiang, H. J.; Lee, H. J. Protein transduction in human cells is enhanced by cell-penetrating peptides fused with an endosomolytic HA2 sequence. *Peptides* **2012**, *37*, 273–284.
- (83) Chen, Y. J.; Deng, Q. W.; Wang, L.; Guo, X. C.; Yang, J. Y.; Li, T.; Xu, Z. S.; Lee, H. C.; Zhao, Y. J. GALA peptide improves the potency of nanobody-drug conjugates by lipid-induced helix formation. *Chem. Commun.* **2021**, *57*, 1434–1437.



JACS Au
AN OPEN ACCESS JOURNAL OF THE AMERICAN CHEMICAL SOCIETY

Editor-in-Chief
Prof. Christopher W. Jones
Georgia Institute of Technology, USA

Open for Submissions

pubs.acs.org/jacsau

ACS Publications
Most Trusted. Most Cited. Most Read.